Remote Sensing of Environment 337 (2026) 115342

Contents lists available at ScienceDirect

Remote Sensing of Environment

journal homepage: www.elsevier.com/locate/rse

# Monitoring water level dynamics in neotropical peatlands with earth observation data

Antje Uhde[a,b,*], Laura L. Hess[c], Alison M. Hoyt[d], Christiane Schmullius[e,b], Euridice N. Honorio Coronado[f], Edmundo Mendoza Olmos[g], Gerardo Flores Llampazo[h], Susan Trumbore[a], Timothy Baker[i], Juan S. Hernandez Suarez[j], Oliver L. Phillips[i], Frederick C. Draper[k], Andrés G. Hernandez Ortega[l], Luis A. Torres-Montenegro[m], R. Scott Winton[g]

[a] Department of Biogeochemical Processes, Max Planck Institute for Biogeochemistry, Hans-Knoell-Str. 10, 07749, Jena, Germany
[b] Department of Earth Observation, Friedrich Schiller University, Jena, Germany
[c] Earth Research Institute, University of California Santa Barbara, Santa Barbara, USA
[d] Department of Earth System Science, Stanford University, Stanford, USA
[e] School for Climate Studies (SCS), Stellenbosch University, Stellenbosch, South Africa
[f] Royal Botanic Gardens Kew, Richmond, UK
[g] Department of Environmental Studies, University of California Santa Cruz, Santa Cruz, USA
[h] Instituto de Investigaciones de la Amazonía Peruana, Iquitos, Peru
[i] School of Geography, University of Leeds, Leeds, UK
[j] Department of Civil and Environmental Engineering, Universidad de los Andes, Bogotá, Colombia
[k] School of Environmental Sciences, University of Liverpool, Liverpool, UK
[l] Facultad de Ciencias Básicas e Ingenierías, Universidad de los Llanos, Villavicencio, Colombia
[m] Herbario Herrerense, Instituto de Investigaciones de la Amazonía Peruana, Iquitos, Peru

## HIGHLIGHTS

- L-band SAR HH backscatter correlates with water level in tropical peatland sites.
- Vegetation structure controls L-band SAR sensitivity to hydrological changes.
- Ecosystems with low vegetation density show strong monitoring potential.
- Palm swamps and flooded forests exhibit good monitoring potential with L-band SAR.
- Our approach supports the integration of peatland hydrology into carbon cycle models.

## ARTICLE INFO

Edited by Dr Marie Weiss

*Keywords:*
Colombian and Peruvian lowland peatlands
L-band SAR
PALSAR-2
GEDI
Hydrological monitoring
Peatland water table

## ABSTRACT

Intact tropical peatlands are globally important carbon stores, yet their hydrology remains poorly understood due to limited accessibility and sparse field measurements. In this study, we evaluate the potential of L-band Synthetic Aperture Radar (SAR) backscatter to monitor above-ground water level variation across diverse lowland peatland ecosystems in Colombia and Peru. Using vegetation structure metrics from GEDI with ancillary remote sensing data, we assess the sensitivity of L-band HH (L-HH) backscatter to water level changes. We observed significant linear correlations between water level and L-HH backscatter in white-sand ecosystems, palm swamp peatlands (open and forested) and seasonally flooded forests. Pole forest peatland water levels showed no correlation with L-HH backscatter. To predict these regressions, we developed ecosystem-specific multiple linear regression models using L-band HV backscatter, NDVI, and GEDI metrics, achieving strong predictive performance ($R^2$ = 0.8–0.94). We further tested the temporal robustness of these relationships by predicting water levels across different years. Our results demonstrate the potential of combining L-band SAR with vegetation metrics derived from spaceborne data for regional monitoring of peatland hydrology. This provides a methodological pathway for integrating tropical peatland dynamics into carbon cycle models.

* Corresponding author at: Department of Biogeochemical Processes, Max Planck Institute for Biogeochemistry, Hans-Knoell-Str. 10, 07749, Jena, Germany.
*Email address:* auhde@bgc-jena.mpg.de (A. Uhde).

https://doi.org/10.1016/j.rse.2026.115342
Received 28 August 2025; Received in revised form 21 February 2026; Accepted 23 February 2026
Available online 3 March 2026

## 1. Introduction

Around one fifth of global peatlands are thought to occur in the tropics (UNEP, 2022), with South America estimated to contribute nearly half of the tropical peatland area (Gumbricht et al., 2017). The importance of peatlands as carbon (C) reservoirs is undisputed (Rieley et al., 2008; Kimmel and Mander, 2010; Goldstein et al., 2020; UNEP, 2022) and studies agree that water levels are the main driver of both greenhouse gas (GHG) fluxes (Hirano et al., 2009; Couwenberg et al., 2010; Hirano et al., 2012; Carlson et al., 2015; Hoyos-Santillan et al., 2019) and peat and C accumulation rates (Cobb et al., 2017; Flores Llampazo et al., 2022). However, knowledge about undisturbed tropical peatland hydrology is limited (Hoyos-Santillan et al., 2019; Apers et al., 2022), which makes it difficult to model peatland C processes.

While intact tropical peatlands are considered a C sink (Lähteenoja et al., 2009; Griffis et al., 2020; Hergoualc'h et al., 2024), carbon dioxide ($CO_2$) emissions have been shown to increase with lowering water levels (Hirano et al., 2009; Hoyos-Santillan et al., 2019; Hoyt et al., 2019), whereas site-scale methane ($CH_4$) emissions, though an order of magnitude lower than $CO_2$ emissions, are highest at above-ground water levels (Hoyos-Santillan et al., 2019; Griffis et al., 2020; Hergoualc'h et al., 2020). Along with water level variation, water source also drives $CH_4$ flux intensity. Neotropical lowland peatland $CH_4$ emissions were shown to be higher in minerotrophic peatlands, i.e., those that receive water input from ground water and/or nearby rivers (Finn et al., 2020).

Hydrology is also a key control on the formation of peat in the tropics. A recent study by Flores Llampazo et al. (2022) assessed water level data at several peat and non-peat wetlands in Peru's Pastaza-Marañón Foreland Basin peatland complex. The authors concluded that the maximum water level depth (i.e., water level below-ground) distinguished peat from non-peat wetlands, with water levels in peat sites being consistently close to the peat surface or above over a two-year study window. The data used in that study were point-scale in-situ water levels, a data source difficult to retrieve given the limited accessibility of tropical peatlands.

Remote sensing offers a unique opportunity for up-scaling field data of different aspects of peatland characteristics to local, regional and even global scales at low cost and effort (Minasny et al., 2023). Optical satellite and airborne imagery have been used to assess temperate and northern peatland hydrology (Kalacska et al., 2018; Burdun et al., 2023). Palomino-Ángel et al. (2024) applied spaceborne laser altimetry to retrieve temperate wetland water levels. In the neotropics, however, dense forest vegetation often restricts the applicability of optical or LiDAR data for such analysis, and field reference data are scarce.

Many studies have successfully used spaceborne Synthetic Aperture Radar (SAR) at L-band wavelength (~23.5 cm) to map flood extent (e.g., Hess et al., 2003; Chapman et al., 2015) and relative water depth (Lee et al., 2015) in tropical forests, where local in-situ information on water level variation was not available, and to map the extent, vegetation type, disturbance level, and peat depth of tropical peat-forming ecosystem types (Draper et al., 2014; Dargie et al., 2017; Bourgeau-Chavez et al., 2021; Hastie et al., 2024; Uhde et al., 2025). Georgiou et al. (2023) integrated in-situ water level measurements with L-band SAR data to estimate water level variation in a tropical forest peatland complex. The authors further combined the water level variation with precipitation data to assess the influence of rainfall on peatland hydrology and thus map ombrotrophic (i.e., precipitation being the main source of water input) and minerotrophic peatlands, but did not account for vegetation structure which affects the SAR backscatter (Wang et al., 1995b; Lee et al., 2015).

The theoretical and demonstrated effectiveness of L-band SAR data as a tool for assessing the hydrology of flood-prone forests stems from its capacity to penetrate vegetation of 50t $ha^{-1}$ up to 100t $ha^{-1}$ biomass, depending on forest structure and heterogeneity (Wang et al., 1995a; Luckman et al., 1997; Saatchi et al., 2011; Mermoz et al., 2014). However, above-ground biomass (AGB) values of over 150t $ha^{-1}$ have been reported for palm swamp and pole forest peatlands, as well as seasonally flooded forests in Peru (Honorio Coronado et al., 2021), challenging the applicability of L-band SAR for hydrological monitoring of forested tropical peatlands.

In this study we use newly collected water level data from wetland sites in Colombia as well as previously published water level data from Peru (Flores Llampazo et al., 2022). These wetlands span a variety of peat-forming ecosystems, characterized by differing hydrology and vegetation structures. These include white-sand ecosystems, palm swamps (open to closed canopy), high-density pole forests and seasonally flooded (floodplain) forests (Honorio Coronado et al., 2021; Flores Llampazo et al., 2022; Winton et al., 2025). Vegetation structure and volume control SAR penetration capabilities, and thus water-level monitoring potential. We first classify the suitable ecosystem structures. We then evaluate the monitoring potential, addressing two research questions: 1) Which peatland ecosystem structures (e.g., low vs. high canopy height, vegetation density) exhibit a statistically significant linear correlation between above-ground water-level variation and L-band HH backscatter, and are thus suitable for remote hydrological monitoring? And 2) To what extent can L-band SAR data, combined with spaceborne vegetation metrics, be used to predict water-level variation across those suitable ecosystems? For reference, we offer a brief description of the water level variation in Colombian sites to align with the information available on Peruvian sites (Flores Llampazo et al., 2022). We then assess the correlation patterns of water level variation and L-band HH backscatter in regard to different vegetation structures in peat and non-peat ecosystems in Colombia and Peru. At the suitable sites, we apply multiple linear regression models to predict the sensitivity of L-band SAR backscatter to changes in water levels. We further test the temporal extrapolation of absolute water level predictions from site levels and conclude with a discussion on the limitations and opportunities of our proposed approach in regard to remote hydrological monitoring and GHG modeling of neotropical peatlands.

## 2. Data and methods

### 2.1. Study area

In this study we focus on tropical lowland peatlands in Colombia (Meta and Guainía departments in the Orinoco basin) and Peru (Loreto department in the Amazon basin; Fig. 1). The peat-forming ecosystems in this region are diverse, and have been mapped using Earth observation data in combination with local field information (Draper et al., 2014; Honorio Coronado et al., 2021; Uhde et al., 2025). Palm swamps are characterized by the dominance of the *Mauritia flexuosa* palm, often mixed with a variable amount of hardwood trees, with canopy heights of around 22m. Open palm swamps feature scattered palms with grass and sedges in between. Pole forests are dominated by thin-stemmed tree species, which are very species-poor but have high vegetation density, and harbor the deepest peat deposits (Draper et al., 2018; Honorio Coronado et al., 2021). Seasonally flooded forests are a more diverse ecosystem consisting mainly of trees (Draper et al., 2018), with similar structure (canopy height, diameter at breast height, basal area) to palm swamps and pole forests (Table 1), and are rarely peat-forming. White-sand ecosystems, only recently described as peat-forming by Winton et al. (2025), have thin-stemmed trees with low canopy height and low vegetation density (Table 1), sometimes sharing the characteristic of dense thin-stemmed trees with pole forests. The largest share of peatlands are palm swamps and seasonally flooded forests (78% in Peru, and 90% in Colombia, Hastie et al. (2022); Uhde et al. (2025)). Pole forests cover 11% of the Peruvian Amazon peatlands (Hastie et al., 2022). In Colombia, white-sand ecosystems cover 4% of the Colombian lowland peatland extent (Uhde et al., 2025; Winton et al., 2025).

Annual precipitation at all sites is above 2500mm. The dry season (monthly precipitation < 100mm) occurs in January in Guainía and from December to February in Meta with minimum water levels occurring

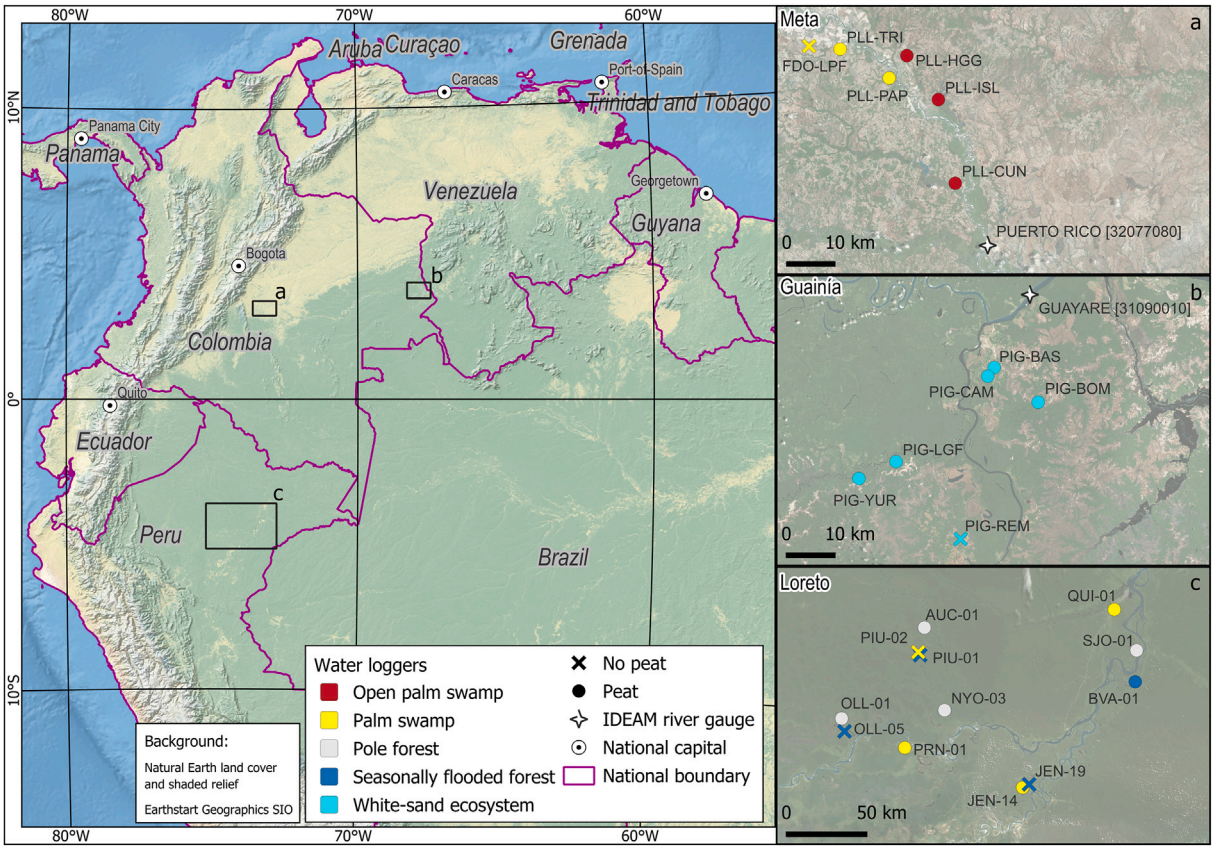


**Fig. 1.** Study area overview with location of in-situ water levels and river gauge stations in the regions of Meta (a) and Guainía (b, Colombia) and Loreto (c, Peru). The color in the insets represents the ecosystem class, while the shape denotes peat presence or absence. (For interpretation of the references to colour in this figure legend, the reader is referred to the web version of this article.)

**Table 1**
Vegetation parameters and ecosystem classes for all sites in Colombia (Guainía, Meta) and Peru (Loreto). Note that we determined a site to contain peat soils and to be a peatland if its surface soils had at least 45% organic matter to a depth of at least 40 cm (Wüst et al., 2003). Peat depths not satisfying this criterion are given in parentheses. AGB = above-ground biomass. AGB values for Loreto plots were taken from Honorio Coronado et al. (2021). Peat depths were determined from soil cores and published in Honorio Coronado et al. (2021) for Loreto, and Winton et al. (2025) for Meta and Guainía plots.

| Site ID | Lat. | Lon. | Ecosystem class | Peat depth [m] | Mean canopy height [m] | Mean diameter at breast height [cm] | Basal area [$m^2$ $ha^{-1}$] | AGB [t $ha^{-1}$] |
|---|---|---|---|---|---|---|---|---|
| PIG-BAS | 3.8 | −67.9 | White-sand Ecosystem | 0.79 | 13.4 | 11 | 2.5 | 15 |
| PIG-BOM | 3.8 | −67.8 | White-sand Ecosystem | 0.95 | 10 | 12.8 | 6 | 26 |
| PIG-LGF | 3.7 | −68.1 | White-sand Ecosystem | 2.1 | 10.4 | 11.1 | 4.4 | 19 |
| PIG-REM | 3.5 | −68.0 | White-sand Ecosystem | (0.31) | 6.7 | 10.1 | 4.5 | 8 |
| PIG-YUR | 3.6 | −68.2 | White-sand Ecosystem | 1.78 | 10 | 15.1 | 4.6 | 17 |
| PIG-CAM | 3.8 | −67.9 | White-sand Ecosystem | 2.1 | 11.1 | 14.2 | 9.9 | 42 |
| AUC-01 | −3.9 | −74.4 | Pole Forest | 8.22 | 24.6 | 19.2 | 30.1 | 245 |
| NYO-03 | −4.4 | −74.3 | Pole Forest | 5.19 | 28.8 | 16.9 | 26.3 | 222 |
| OLL-01 | −4.4 | −74.8 | Pole Forest | 3.27 | 19.9 | 15.5 | 24.3 | 184 |
| SJO-01 | −4.1 | −73.2 | Pole Forest | 5.56 | 19.9 | 12.4 | 24.9 | 209 |
| JEN-14 | −4.8 | −73.8 | Palm Swamp | 1.61 | 21.7 | 23.3 | 27.5 | 202 |
| PRN-01 | −4.6 | −74.5 | Palm Swamp | 1.1 | 21.8 | 21.9 | 30 | 229 |
| QUI-01 | −3.8 | −73.3 | Palm Swamp | 3.39 | 16.5 | 14.4 | 23.2 | 142 |
| PIU-02 | −4.1 | −74.4 | Palm swamp | (0.0) | 25.5 | 21.1 | 34 | 286 |
| PIU-01 | −4.1 | −74.4 | Seasonally Flooded Forest | (0.0) | 27.2 | 20.4 | 21.9 | 225 |
| JEN-19 | −4.8 | −73.8 | Seasonally Flooded Forest | (0.0) | 23.7 | 22.5 | 25.7 | 260 |
| BVA-01 | −4.2 | −73.2 | Seasonally Flooded Forest | 4.0 | 10 | 13 | 21.5 | 175 |
| OLL-05 | −4.5 | −74.8 | Seasonally Flooded Forest | (0.0) | 19.4 | 18.6 | 21.9 | 201 |
| PLL-HGG | 3.3 | −73.4 | Open Palm Swamp | 5.89 | 7.9 | 22.1 | 11.4 | 28 |
| PLL-CUN | 3.1 | −73.3 | Open Palm Swamp | 2.85 | 5.29 | 8.63 | 0.64 | 2 |
| PLL-ISL | 3.2 | −73.3 | Open Palm Swamp | 3.98 | 4.01 | 24.71 | 5.08 | 5 |
| PLL-PAP | 3.3 | −73.4 | Palm Swamp | 6.4 | 17.5 | 23.2 | 33.6 | 272 |
| FDO-LPF | 3.3 | −73.5 | Palm Swamp | (0.2) | 12 | NA | NA | NA |
| PLL-TRI | 3.3 | −73.5 | Palm Swamp | 3.17 | 18.47 | 24.41 | 21.33 | 172 |

between February and April. Loreto lacks a distinct dry season and experiences the lowest water levels between August and October (Flores Llampazo et al., 2022).

### 2.2. In-situ data

#### 2.2.1. Site water levels

Water levels at the Peruvian sites were recorded in individual dip wells at point-scale in continuous 30-minute intervals between 12/2017 and 07/2020, using automated pressure loggers. The pressure measurements were corrected for water level depth with in-situ barometric data and manual measurements of water level height (Flores Llampazo et al., 2022). For water level measurements in Colombia we followed a similar setup, with continuous monitoring at each site using automated pressure loggers in perforated PVC tubes (Model 3001 Levelogger 5, Solinst Canada Ltd.), and data recorded at 30-minute intervals from 02/2023 to 03/2025. All loggers were installed at depths consistently below the water table. We anchored the wells using a bentonite seal at the surface. We measured the initial water level in the field with a tape measure for calibration of water level relative to the ground. Due to poor weather conditions in the field and data quality concerns, we excluded the time-series starting from February 2024 for sites PIG-LGF and PIG-REM, from August 2024 for site PLL-PAP, and from November 2024 for sites PIG-YUR and PIG-CAM. At least 12 months of usable data were preserved for each of these sites. As our in-situ barometric logger failed in the Meta region, we assessed the ERA5 surface pressure (Hersbach et al., 2020) and found good correlation with the in-situ barometric pressure available in Guainía ($\rho$ = 0.97). We thus used the ERA5 surface pressure to correct both the Guainía and Meta data for barometric pressure, to be consistent within the Colombia sites. In this paper, we discuss water level height with positive values when above-ground and negative values when below-ground.

#### 2.2.2. Vegetation structure

Forest plot data for Colombian sites were collected during field campaigns in 2022 and 2023 (Winton et al., 2025). All trees and palms with a stem diameter at breast height (DBH) > 10 cm were measured in diameter and height, and the canopy height of each palm and tree was estimated in the field using a clinometer. For the non-peat palm swamp site FDO-LPF, only mean canopy height data are available. We calculated above-ground biomass (AGB) for tree species using the allometric eq. (1) by Chave et al. (2014). We extracted South America mean wood density values for each species from the Global Wood Density Database (Zanne et al., 2009). If species data were unavailable, we calculated the mean of the genus wood density, the family, and if that was also unavailable, or for unidentified individuals, we used the mean wood density of the plot.

$$AGB = 0.0673^{*}(\rho^{*} dbh^{2*} H)^{0.976} \quad (1)$$

with $AGB$ = above-ground biomass, $\rho$ = wood density (g/cm$^3$), $dbh$ = diameter at breast height, and $H$ = tree height. For palm species, we used the species-specific allometric equations and dry mass fractions from Goodman et al. (2013) (Eq. (2) for *M. flexuosa* and Eq. (3) for *Mauritiella*). For individual *M. flexuosa* palms shorter than 9m (shortest total *M. flexuosa* height used in Goodman et al. (2013)), and *Mauritiella* individuals shorter than 5m (shortest *Mauritiella* height used in Goodman et al. (2013)), we used the family equation (Eq. 4).

$$AGB = -261.1 + 39.068 * H \quad (2)$$

$$AGB = 1.2912 * log(H) \quad (3)$$

$$AGB = exp(-3.0883 + 1.0311 * log(dmf * dbh^2 * H)) \quad (4)$$

with $AGB$ = above-ground biomass, $H$ = total palm height, $dmf$ = dry mass fraction, and $dbh$ =diameter at breast height. We then converted the kg per plot (0.1ha) to t ha$^{-1}$ by dividing by 100.

We retrieved 2017 census data for the Peruvian sites from the ForestPlots.net Database (ForestPlots.net; ForestPlots.net et al., 2021; Lopez-Gonzalez et al., 2011). We averaged the data at each site to determine site mean canopy height, mean DBH, the slope of the DBH size frequency distribution, and basal area (BA, the total cross-sectional area of tree trunks per unit area (Bettinger et al., 2017)), and extracted the maximum DBH at each site. The individual forest plots are between 0.1 and 1ha (Honorio Coronado et al., 2021; Winton et al., 2025). The AGB values for Peruvian sites were taken from Honorio Coronado et al. (2021).

#### 2.2.3. Hydrological data

For the Colombian regions of Guainía and Meta, we downloaded all available river gauge data from the stations Guayare [31097010] (1984-2025, 3.96°, −67.83°) and Puerto Rico [32077080] (1979-2025, 2.94°, −73.21°), from the Colombian Institute of Hydrology, Meteorology and Environmental Studies (IDEAM, 2024). Additionally, we used daily precipitation from the MSWEP dataset (Beck et al., 2019) overlapping with the water level acquisition periods, to correlate precipitation at the Colombian sites with site water level. We used these data to 1) assess the correlation between site and river water level and precipitation, and 2) discuss the hydrological context of the study period in comparison to long-term average low water (March and April) and high water (July and August) river levels. A similar analysis for Peruvian sites is presented in Flores Llampazo et al. (2022).

### 2.3. Earth observation data

#### 2.3.1. PALSAR-2 data

PALSAR-2, an L-band SAR satellite launched by Japan's Aerospace Exploration Agency (JAXA) in 2014, employs a systematic observation strategy designed to acquire nearly wall-to-wall coverage of tropical/subtropical and boreal regions in wide-swath (350 km) ScanSAR mode (Rosenqvist et al., 2014). We obtained PALSAR-2 ScanSAR data (level 2.2) via Google Earth Engine (GEE, (Google for Developers, 2024)) for the period 08/2014-04/2025. The data have a spatial resolution of 25m × 25m and a temporal revisit cycle of 42 days, though some acquisitions are missing. We assessed all available orbits separately to account for differences in ScanSAR incidence angle (each orbit with a consistent incidence angle) and used only orbits with > 3 acquisitions overlapping each site's water level data recording periods. The incidence angles range from 27°-50° (Tab. S1), which have been shown to introduce variations in HH (hereafter L-HH) backscatter of up to 3dB in flooded vegetation (Chapman et al., 2015). We calculated spatial mean values (Section 2.4) on linear data and subsequently scaled them to dB. We used the L-HH spatial mean backscatter for individual acquisitions that overlapped with the water level measurements to assess correlation (Section 2.5). We further averaged the spatial mean dB backscatter over the entire time-series of each site and orbit (temporal mean), and calculated the temporal standard deviation for L-HH and HV (hereafter L-HV) polarizations.

#### 2.3.2. GEDI data

The Global Ecosystems Dynamics Investigation (GEDI) instrument is a waveform LiDAR aboard the International Space Station. It acquires vegetation vertical structure information of tropical and temperate forests at a 25m footprint level (Dubayah et al., 2020). We used GEDI Level 2A and 2B data to extract vegetation structure metrics, including relative height percentiles (e.g., rh95, rh50, rh95-rh50), total canopy cover (TCC), and foliage height diversity (FHD). The data were acquired between 2019 and 2022, with acquisition dates and seasons varying by site (Tab. S2). Where more than one footprint was available per site (Section 2.4), we averaged all available footprints. We supplemented missing values for white-sand ecosystem sites PIG-REM, PIG-BAS, and FDO-LPF (palm swamp) with in-situ forest plot measurements; rh50 was replaced by canopy height/2, and TCC and FHD were modeled by using all available vegetation data for the same ecosystem.

We found low to moderate Pearson's correlation coefficients between spaceborne and in-situ vegetation parameters ($\rho \leq 0.76$ for correlations of in-situ canopy height, DBH, and number of trees per ha with GEDI rh50, rh95, TCC, and FHD), except for in-situ basal area, which reached $\rho > 0.8$ for all GEDI parameter correlations (Fig. S1, Fig. S2). We focused on using spaceborne data because it offers transferability to other, non-censused regions, but additionally assessed in-situ data to improve model performance.

#### 2.3.3. Ancillary remote sensing products

Frequent cloud cover poses a challenge to using optical remote sensing products in the Western Amazon region. The Landsat program provides an archive of optical imagery dating back to the early 1970s (Loveland and Dwyer, 2012). The Landsat 8 satellite was launched in 2013, equipped with a sensor featuring nine spectral bands covering the visible, near- and shortwave infrared, and a revisit time of 16 days at the equator (Irons et al., 2012). We applied the provided default cloud mask to all images with a maximum of 25% cloud cover in the Landsat 8 archive (until October 2024) covering our sites, and calculated the spatial mean Normalized Difference Vegetation Index (NDVI, (Rouse et al., 1974)). Given the low availability of cloud-free acquisitions, we then averaged the NDVI across all available acquisitions (Tab. S2), regardless of season to increase the number of NDVI values and decrease the influence of outliers caused by cloud shadows and other potential brightness errors that were not accounted for individually.

The Copernicus Sentinel-2 mission of the European Space Agency and European Commission is a multi-spectral Earth observation mission, designed for operational monitoring of the Earth's surface (Drusch et al., 2012), first launched in 2015. We created dry and wet season false-color composites (bands 12-8-4, Tab. S3) for each region (Meta, Guainía and Loreto). We applied histogram stretching to the Sentinel-2 composites and stored the data in byte format for our image segmentation (Section 2.4).

### 2.4. Segmentation

As the water level measurements consist of point-scale data, some method of up-scaling to Earth observation data is necessary. Instead of conducting a per-pixel analysis, we computed spatial mean values of the Earth observation data for image objects (polygons) containing the in-situ water level points (Fig. 2), to reduce the speckle effect in SAR data and increase the number of available GEDI footprints. Although both the in-situ forest plots and the image objects contain the respective water level point location, the two don't necessarily fully overlap as the forest plots were set up in a specific pattern on the ground, while the polygons follow Earth observation pixel outlines around a homogeneous area. Our analysis is based on the polygons, while we use the average forest plot parameters as a reference to in-situ vegetation structure (Section 2.2.2). The mean polygon size is 48.5ha (3.2 - 203.8ha). Our multi-resolution segmentation process in eCognition (Trimble Germany GmbH, 1995-2022) incorporated relative terrain height (Hess and Durieux, 2026) derived from the Copernicus DEM (Copernicus Contributing Missions Online, 2022), and the Sentinel-2 dry and wet season false-color composites, and aimed at generating polygons of homogeneous land cover. We adapted the segmentation parameters for each region, as they are relative to the size of the spatial extent used for the segmentation (Tab. S3). We verified the outline of each polygon by comparing them with high-resolution optical satellite images and using our field knowledge of the sites.

### 2.5. Site filtering

For each site, we defined correlation patterns between the individual acquisition's L-HH backscatter and site water levels (daily mean of the PALSAR-2 acquisition dates) to be either linear, exponential, logarithmic or none, based on statistical analysis of the two time-series (Fig. S3, Fig. S4). We chose a water level threshold of −10 cm, as this was the threshold of linear correlations between water level and L-HH backscatter. The soil penetration depth of the L-HH SAR signal depends primarily on soil moisture and surface roughness, with decreasing penetration as either soil moisture or surface roughness increases, and is estimated to be a few to 20 cm for non-arid mineral soils (Ulaby et al., 1996; Kojima et al., 2016; Zhou et al., 2025). Very few field or modeled penetration depth estimates are available, however, for peat soils. Georgiou et al. (2023) found that L-HH sensitivity extended to 15 cm below the surface for peat soils of the Congo basin. For our sites, soil water depths below −10 cm were not detectable with L-HH. Furthermore, the tropical peat surface consists of a micro-topography of hummocks and hollows, and it is possible that the position of the dip well lies above the mean peat surface when considering the extent of the Earth observation pixels (Georgiou et al., 2023). We applied a Principal Component Analysis to standardized variables (i.e., correlation-based PCA, 2 components) focused on vegetation parameters (L-HV temporal mean and standard deviation, NDVI and GEDI L2A rh95) to distinguish sites with linear L-HH backscatter-water level correlations from those with nonlinear or no correlation.

The first two principal components explained 91% of the dataset variance, and two primary clusters of linear correlation emerged (Fig. 3):

1. Low-statured white-sand ecosystems.
2. Tall, dense forests, including palm swamps and seasonally flooded forests.

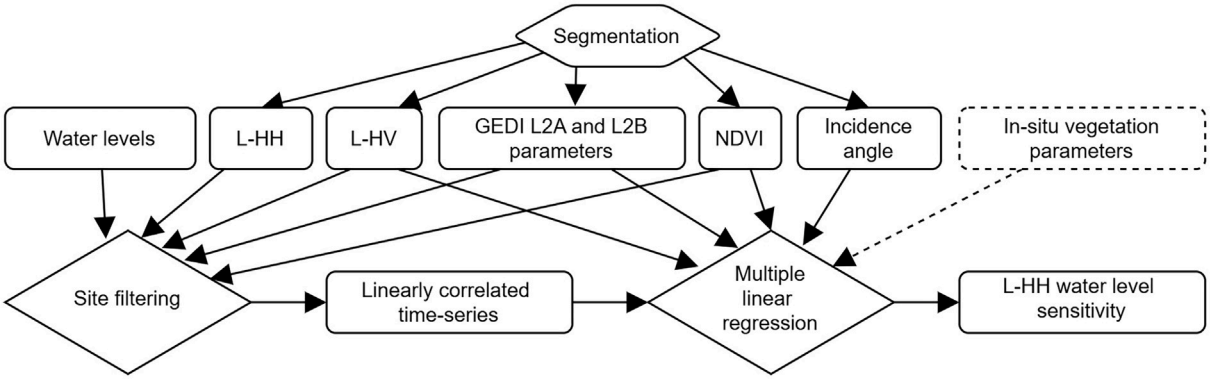


**Fig. 2.** Study workflow, from a segmentation into image objects to a filtering of linearly correlated sites based on vegetation structure parameters and the prediction of L-HH sensitivity to changes in water level using multiple linear regression. The dashed lines indicate parameters that were tested in addition to the parameters with solid lines.

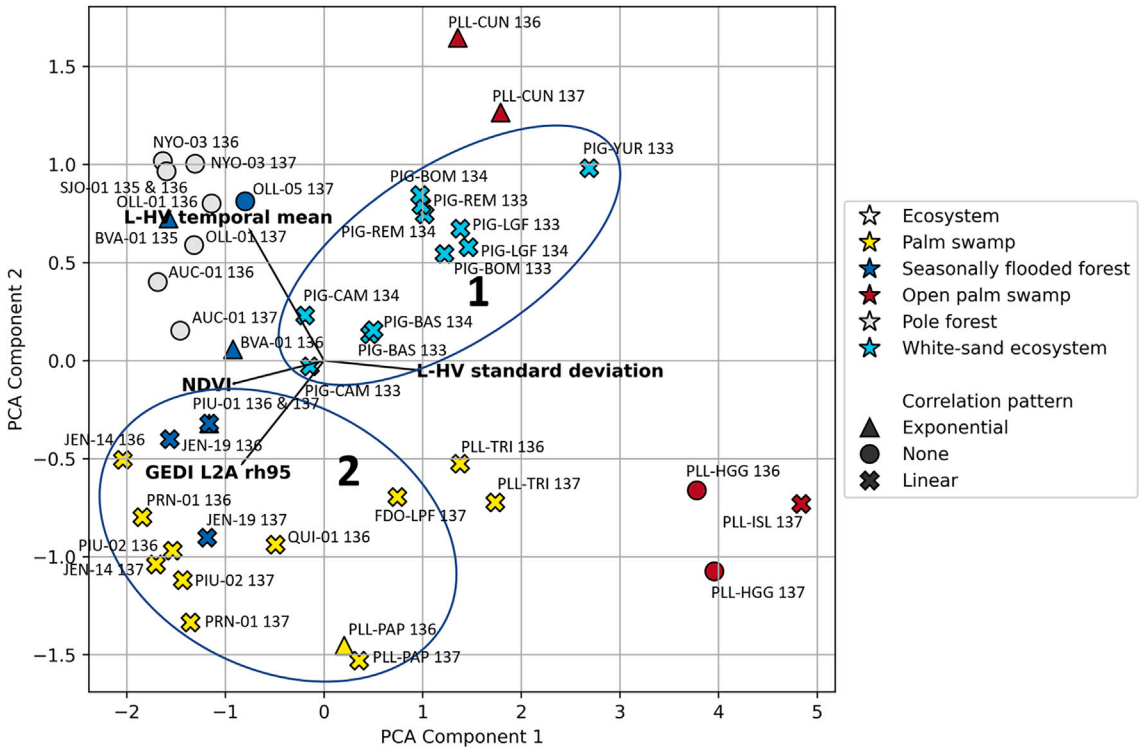


**Fig. 3.** Principal Component Analysis with two principal components, based on vegetation greenness (NDVI), canopy height (GEDI L2A r95), vegetation density (L-HV temporal mean) and variation in vegetation density (L-HV standard deviation). The color indicates the ecosystem class, while the shape marks the correlation pattern (exponential, linear or no correlation). Each marker is labeled with its site code and PALSAR-2 orbit number. (For interpretation of the references to colour in this figure legend, the reader is referred to the web version of this article.)

The palm swamp site PLL-TRI, though classified as palm swamp, is structurally between an open and a dense palm swamp (Fig. 3). The site has a similar basal area to palm swamp QUI-01 despite a larger DBH, given there are less than half as many palms present in PLL-TRI. The site was excluded from this analysis to focus on densely forested swamps in cluster 2. A potential additional cluster, consisting of open palm swamps, lacked sufficient data points for further statistical analysis.

### 2.6. Multiple linear regression

To predict the L-HH water level sensitivity (i.e., the slope of the linear regression) of each site based on Earth observation data, we developed one multiple linear regression model for each cluster. We applied an interquartile-range outlier filter based on regression slopes to both clusters, which excluded a site with an exceptionally high regression slope value (seasonally flooded forest site JEN-19 with > 1m increase in water level needed for 1dB increase in L-HH backscatter, Fig. 5(b) from cluster 2. The independent variables varied slightly between clusters:

- Cluster 1: PALSAR-2 incidence angle, L-HV temporal mean and standard deviation, NDVI, GEDI L2A rh95, rh50, and rh95-rh50.
- Cluster 2: PALSAR-2 incidence angle, L-HV temporal mean, NDVI, GEDI L2A rh95, and GEDI L2B TCC and FHD.

We assessed model performance using leave-one-out cross-validation. Validation metrics included Mean Absolute Error (MAE), Mean Squared Error (MSE), and $R^2$. An $R^2$ threshold of 0.5 was used to determine acceptable predictions. MAE values were interpreted relative to the range of standard errors of the individual linear regressions, with acceptable performance when MAE remained within this range. The standard errors of the individual linear regressions in cluster 1 range from 0.46 cm–2.21 cm, thus an MAE of $\leq$ 2.21 is acceptable for model 1. In cluster 2, standard errors reach 19.31 cm, raising the acceptable MAE for model 2. MSE was evaluated against the variance (average of the squared deviations from the mean slope) in observed slope values, which is 13.3 in cluster 1 and 252.51 in cluster 2. An MSE value smaller than the variance is acceptable.

### 2.7. Temporal extrapolation

We tested temporal extrapolation only for sites with at least two full years of water level data, and where both years individually showed significant linear correlations between water level and L-HH backscatter at the same PALSAR-2 orbit (i.e., 2018 and 2019 for Peru, 2023 and 2024 for Colombia). We trained linear regression models on one year and predicted water levels for the remaining PALSAR-2 acquisition dates of that site. The accuracy of these predictions was assessed using RMSE, MAE and $R^2$. An $R^2$ threshold of 0.5 was used to indicate acceptable predictions. We compared the RMSE and MAE to the standard deviation $\sigma$ of the water level data and accepted a model if MAE was smaller than RMSE and RMSE was smaller than $\sigma$.

## 3. Results

### 3.1. Colombian peatland hydrology

Water levels in Colombian peat and non-peat wetlands show distinct variations between seasons (Fig. S8), following regional river gauge levels (Pearson's correlation coefficient $\rho$ = 0.73 for peat sites, $\rho$ = 0.59 for non-peat wetlands). However, during the 2023/2024 hydrological year, river levels were lower than average (strong El Niño year, i.e., drier than average), with the mean high water river level (July and August 2023) 0.76m and 0.22m lower than the long-term average high water level at Guayare and Puerto Rico stations, respectively (IDEAM, 2024). The mean low water level (March and April 2024) at Puerto Rico station was 0.56m below the long-term mean low water level while it showed no difference from the long-term mean low water level at Guayare station. In contrast, the correlation with daily precipitation

**Table 2**
Hydrological statistics of Colombian sites. The lowest and highest water level are given in reference to the peat/ground surface and are taken from the entire available water level time-series of each site. Positive water level values refer to a water table above-ground and negative values refer to a water table below-ground. To account for the different lengths of water level time-series available for the different sites, we only used data from February 2023 to February 2024 (12 months) to calculate the percentage of time the water level is above-ground.

| Site | Ecosystem class | Peat site | Lowest water table [m] | Highest water table [m] | Percentage of time water level is above-ground [%] |
|---|---|---|---|---|---|
| PIG-BAS | White-sand Ecosystem | yes | 0.201 | 0.719 | 100 |
| PIG-BOM | White-sand Ecosystem | yes | −0.325 | 0.213 | 50 |
| PIG-LGF | White-sand Ecosystem | yes | −0.098 | 0.093 | 71 |
| PIG-REM | White-sand Ecosystem | no | −0.369 | 0.180 | 42 |
| PIG-YUR | White-sand Ecosystem | yes | −0.167 | 0.396 | 23 |
| PIG-CAM | White-sand Ecosystem | yes | 0.034 | 0.336 | 100 |
| PLL-HGG | Open Palm Swamp | yes | −0.177 | 0.341 | 67 |
| PLL-CUN | Open Palm Swamp | yes | −0.027 | 1.491 | 97 |
| PLL-ISL | Open Palm Swamp | yes | −0.416 | 0.972 | 74 |
| PLL-PAP | Palm Swamp | yes | −0.169 | 0.989 | 92 |
| FDO-LPF | Palm Swamp | no | −0.024 | 0.136 | 97 |
| PLL-TRI | Palm Swamp | yes | −0.034 | 0.254 | 96 |

was weaker ($\rho$ = 0.22 for peat sites, $\rho$ = 0.24 for non-peat wetlands). Although this lack of correlation does not imply precipitation is not an important water source, it suggests that groundwater and lateral flow play an important role in site hydrology.

All sites maintained water levels above-ground over 50% of the time, except for the white-sand ecosystem sites PIG-REM (42%) and PIG-YUR (23%). The open palm swamp site PLL-ISL showed the lowest minimum water levels (−0.416m), followed by the non-peat white-sand ecosystem site PIG-REM (−0.369m, Table 2). Two white-sand ecosystem sites had water levels continuously above-ground throughout the entire study period. The largest variation in water levels (> 1.5m) was observed in the open palm swamp PLL-CUN (Table 2).

### 3.2. Correlations of l-HH and water level variation

We found significant linear correlations ($p \leq 0.05$) between site above-ground water levels and L-HH backscatter at 16 sites (with 1–2 PALSAR-2 orbits each), independent of peat occurrence. Only three site-orbit combinations showed an exponential correlation (Fig. S3, Fig. S4). All Peruvian pole forest water levels showed no correlation with the L-HH backscatter. Our PCA further reveals that all pole forest sites cluster around constant, high L-HV temporal mean backscatter (Fig. 3), indicating high vegetation volume with little seasonal variation. In the white-sand ecosystems (cluster 1), we observed linear correlations in sites with increased L-HV temporal mean backscatter and L-HV standard deviation. The sites in cluster 1 show higher L-HH sensitivity (i.e., lower slope of linear regression or simply less change in water level needed for a change in L-HH backscatter) to water level variation than sites in cluster 2, with lower canopy height and NDVI values, but relatively high L-HV backscatter and standard deviation (Tab. S4). The linearly correlated palm swamp and seasonally flooded forest sites (cluster 2, low and medium L-HH sensitivity) have medium to high canopy height values (GEDI L2A rh95), and distinctively lower L-HV temporal mean backscatter than the pole forests (no linear correlation, Fig. 3, Tab. S4 “None (high vegetation density)”. Altogether, the observed variability in L-HH sensitivity and correlation type aligns with distinct site characteristics defined by vegetation structure and not solely by ecosystem class.

### 3.3. Monitoring water level change with SAR

The multiple linear regression model of cluster 1 demonstrated strong predictive performance for estimating water level sensitivity

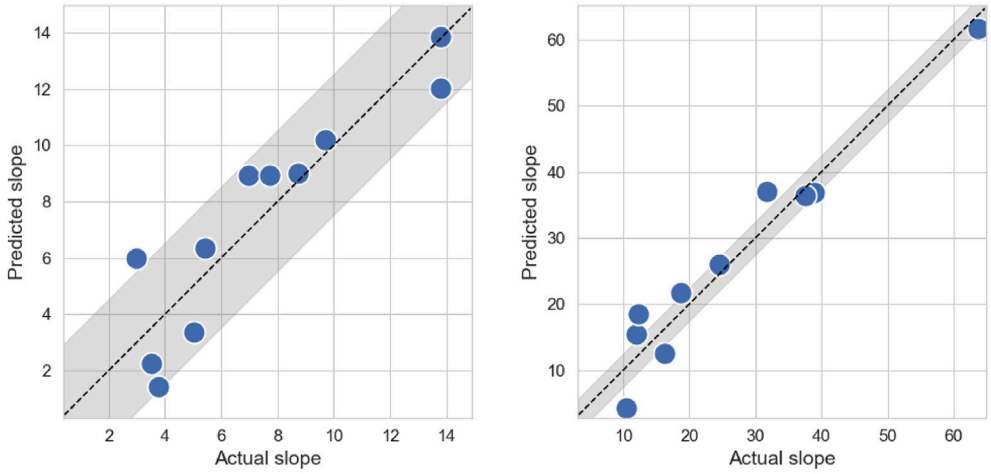


(a) (b)

**Fig. 4.** Results of the multiple linear regression predicting the slope of linear regressions (i.e., L-HH sensitivity) for cluster 1 (Fig. 4(a), $R^2 = 0.8$) and cluster 2 (Fig. 4(b), $R^2 = 0.94$). The grey band represents 2.5 cm above and below the dashed 1:1 line. Cluster 1 has lower slope values (L-HH sensitivity is higher, i.e., steeper increase in L-HH backscatter with water level increase than in cluster 2), and lower range of slope values, as indicated by the different axis scales in the two figures. While cluster 1 consists of white-sand ecosystems with low-statured trees and low vegetation density, cluster 2 contains palm swamps and seasonally flooded forests of high canopy height and above-ground biomass (Table 1, Fig. 3). Both multiple linear regressions fulfill the three acceptance criteria defined in 2.4. (For interpretation of the references to colour in this figure legend, the reader is referred to the web version of this article.)

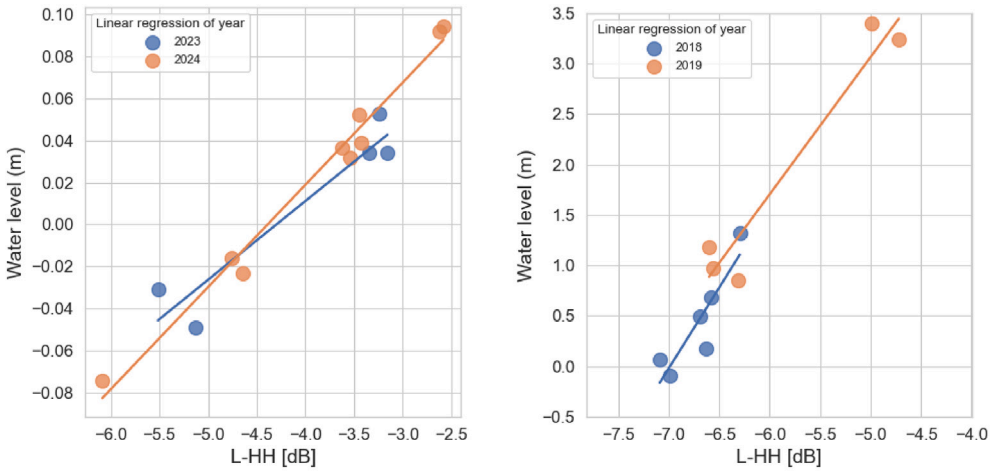


(a) (b)

**Fig. 5.** Linear regression of individual years of water levels and L-HH acquisitions for site PIG-BOM orbit 134 (white-sand ecosystem) with good temporal extrapolation results when using one year's regression to predict the other year's water levels (Fig. 5(a), and site JEN-19 orbit 137 (Fig. 5(b), seasonally flooded forest) where the 2019 water level is much higher that in 2018. (For interpretation of the references to colour in this figure legend, the reader is referred to the web version of this article.)

from remote sensing data (Fig. 4(a), with an MAE of 1.37 cm, an MSE of 2.61 $cm^2$, and an $R^2$ of 0.8, thus meeting all three acceptance criteria (as defined in 2.6). The strongest predictor variables for cluster 1 were the GEDI L2A rh50, the difference between rh95 and rh50 (rh95-rh50), and L-HV standard deviation. The individual variation of each predictor variable with the slopes in cluster 1 is shown in Fig. S5.

Cluster 2 resulted in an MAE of 3.47 cm, MSE of 15.27 $cm^2$, and an $R^2$ of 0.94, also meeting all three acceptance criteria (Fig. 4(b). The strongest predictor variables for cluster 2 were the GEDI L2A rh95, L2B FHD and the PALSAR-2 temporal mean HV backscatter (Fig. S6).

In cluster 1, model performance improved to an MAE of 0.39 cm, MSE of 0.21 $cm^2$ and $R^2$ of 0.98 when we replaced the GEDI L2A rh95 with the in-situ canopy height (Fig. S7a). This was the opposite case in cluster 2, where the model failed all three acceptance criteria (MAE = 23.43 cm, MSE = 1067.82 $cm^2$, and $R^2 = -3.23$, Fig. S7b). Although the in-situ canopy height and GEDI L2A rh95 correlate moderately well ($\rho$ = 0.77, Fig. S1), GEDI seems to underestimate canopy height at sites with high in-situ canopy height values (Fig. S2). The additional use of other in-situ vegetation parameters such as DBH, basal area or slope of the size distribution function did not improve model performance further.

### 3.4. Temporal extrapolation potential

From all 21 linear 2-year time-series (16 sites with 1–2 PALSAR-2 orbits each), four individual site-orbit combinations provided significant linear correlations for both years of water level data independently ($p \leq 0.05$, Table 3). We used a linear regression for each of these years to predict the water levels of the remaining PALSAR-2 acquisition dates of each site-orbit combination. For all sites, RMSEs were greater than MAEs and all $R^2$ values are above 0.5. The best results were obtained for PIG-BOM (Fig. 5(a), white-sand ecosystem), PIG-BAS (white-sand ecosystem), and QUI-01 (palm swamp), where the models achieved an MAE and RMSE below $\sigma$ and an $R^2$ above 0.5 for both, forward and backward predictions (2023 and 2024 in the Guainía region and 2018 and 2019 in the Loreto region). JEN-19 (seasonally flooded forest, Fig. 5(b) has an RMSE and MAE above $\sigma$ when using 2018 data to predict 2019 water levels (Table 3) and the largest $\sigma$ of all sites for the linear regression of 2019 data.

**Table 3**
Results of temporal extrapolation of significant linear regressions using a single year ("Training year") to predict water levels of the remaining PALSAR-2 acquisition dates ($\sigma$ = standard deviation, RMSE = Root Mean Squared Error, MAE = Mean Absolute Error).

| Site | Orbit | Ecosystem class | Training year | $\sigma$ | RMSE | MAE | $R^2$ |
|---|---|---|---|---|---|---|---|
| PIG-BAS | 134 | White-sand Ecosystem | 2023 | 10.95 | 7.92 | 5.62 | 0.73 |
| PIG-BAS | 134 | White-sand Ecosystem | 2024 | 15.81 | 6.13 | 5.28 | 0.77 |
| PIG-BOM | 134 | White-sand Ecosystem | 2023 | 4.52 | 1.82 | 1.52 | 0.9 |
| PIG-BOM | 134 | White-sand Ecosystem | 2024 | 5.51 | 1.61 | 1.39 | 0.91 |
| QUI-01 | 136 | Palm Swamp | 2018 | 8.31 | 5.06 | 4.42 | 0.71 |
| QUI-01 | 136 | Palm Swamp | 2019 | 10.49 | 5.46 | 4.54 | 0.52 |
| JEN-19 | 137 | Seasonally Flooded Forest | 2018 | 51.61 | 70.42 | 59.93 | 0.57 |
| JEN-19 | 137 | Seasonally Flooded Forest | 2019 | 127.79 | 57.77 | 43.96 | 0.60 |

## 4. Discussion

### 4.1. Site hydrology

Our site water level analysis highlights hydrological differences between peat and non-peat ecosystems. The open palm swamp site PLL-ISL had the lowest overall water levels in Colombia. At this site, we observed a complex landscape of floating peat mats in the field, which we did not find at any other site, making comparisons to other sites difficult. The non-peat white-sand ecosystem site PIG-REM had water tables below 35 cm below-ground, supporting the hypothesis of Flores Llampazo et al. (2022), that hydrology is a dividing factor between peat presence and absence. The water levels in the non-peat palm swamp FDO-LPF, however, did not drop lower than a few cm below the peat surface. In the field, we observed a layer of organic soil 20 cm thick at this site (Table 1), which did not satisfy our definition of a peatland ($\geq$ 40 cm organic soil). This site could be in an early stage of peat development, which would explain its hydrological similarities to peat palm swamps; however, confirmation of this hypothesis requires

more field data. Disturbance was not observed in the field. Similarly, the influence of extreme climate events such as the El Niño-Southern Oscillation (ENSO) needs further investigation. In the sites investigated in this study, El Niño (2023/2024 in Colombia) usually leads to drier-than-average dry seasons, whereas La Niña results in higher water levels in the wet season (see 3.1). Although the recorded water levels cover an El Niño year, additional years of water level data are necessary to assess long-term water level variation and the effect of ENSO on the hydrology of Colombian lowland peatlands.

### 4.2. Opportunities and limitations of proposed monitoring approach

Our study demonstrates a high potential for integrating L-band SAR data with vegetation structure metrics to monitor neotropical lowland peatland hydrology dynamics. Vegetation structure and density (AGB) influence the applicability of the proposed approach. We found sites less green (low NDVI compared to other sites), with medium-to-high vegetation density (L-HV backscatter), and variation in such (L-HV standard deviation), to be most conducive to monitoring water level dynamics with Earth observation data using linear regression, across the entire range of forest height (GEDI L2A rh95, Tab. S4). The L-HH backscatter did not correlate with water level variation in any of the pole forest sites. We attribute this partly to the low above-ground water level variation in pole forest ecosystems, which exhibit maximum water levels of 0.19 cm to 0.45 cm above ground (Flores Llampazo et al., 2022). With only small changes in water level, the difference in L-HH backscatter is minimal. At three of the Colombian sites, however, we recorded maximum water levels of less than 20 cm as well (Table 2). All of these Colombian sites have a vegetation structure distinct from that of the pole forests (Fig. 3), as well as lower biomass (Table 1). Thus, we can assume that the high vegetation volume hinders the applicability of the L-band SAR wavelength for hydrological monitoring of pole forest peatlands, as they have the highest L-HV backscatter of all sites observed (Fig. 3). The increased standard errors and variance in significant linear regressions of dense swamp (high AGB) water levels with L-HH backscatter (cluster 2), compared to less dense white-sand ecosystems of cluster 1, further support this theory (see also Fig. S9). A longer wavelength with increased penetration capacity and sensitivity to higher AGB ecosystems, such as the P-band of the BIOMASS SAR mission with a wavelength of around 70 cm (Le Toan et al., 2011), launched in April 2025, would likely provide valuable data for hydrological characterization of dense tropical wetland ecosystems. The P-band wavelength is expected to saturate above AGB volumes of 200t $ha^{-1}$ (Saatchi et al., 2011), making it highly relevant for many of our study sites. However, systematic, operational coverage is necessary for continuous monitoring, which is currently not provided by the BIOMASS mission.

Additionally, sensor parameters play an important role in the applicability of our proposed approach. When assessing correlation patterns between linearly and non-linearly correlated sites (Section 2.5), some separability constraints remained, regardless of vegetation parameters used in the PCA. This might be partially explained by incidence angle, as for example PLL-PAP (palm swamp) shows a linear correlation at 37° incidence angle (orbit 137) but not at 49° (orbit 136). According to both canopy backscatter modeling (Wang et al., 1995b) and empirical studies (Tsyganskaya et al., 2018; Oakes et al., 2024), targets imaged at larger incidence angles (with pixels located further away from the nadir point of the satellite) experience higher signal attenuation, owing to the greater path length through the vegetation canopy. However, since canopy attenuation is also influenced by canopy density and depth, for stands with open canopies the flooding signal reduction at shallow incidence angles may be minimal (Tsyganskaya et al., 2018). In our study, PLL-TRI (palm swamp) shows a linear correlation at an incidence angle of 49°, though with lower AGB (Table 1). PRN-01 and PIU-02 (palm swamps with similar AGB but shorter palms, Table 1) show linear correlations between water level and L-HH backscatter at 45°. We therefore cannot clearly identify a single incidence angle threshold for the sensitivity of L-HH backscatter to above-ground water level changes for the wide range of neotropical peat forest types and structures. Observations of L-HH backscatter differences at the same site with similar water levels but using different incidence angles could result in a false positive interpretation of water level change. This highlights the importance of using consistent incidence angles when monitoring tropical forest peatland above-ground water levels. Alternatively, backscatter thresholds can be adjusted for larger incidence angles (e.g., ScanSAR angles > 40°; Oakes et al. (2024)). The improved temporal coverage provided by the NISAR L-band SAR satellite mission launched in July 2025, with a 12-day revisit cycle at identical incidence angles (NISAR, 2018), will improve representation of short-term water level variations, as well as increase the chances of capturing the total range of water levels (Fig. S8).

In-situ information is important in the interpretation of the results, but only partly improved the water level modeling. Our remote sensing data-based PCA showed the separability of two distinct clusters with linear correlations, composed of white-sand ecosystems in one and palm swamps and seasonally flooded forests in the other. It further separated sites with non-linear or no correlation, such as pole forest ecosystems from white-sand ecosystems (Fig. 3). The open palm swamp sites were distributed across different characteristics of the PCA. Although no palms were recorded at the open palm swamp site PLL-CUN (making it structurally similar to white-sand ecosystem sites, Fig. 3), it is floristically similar to other open palm swamp sites (Winton et al., 2025), and palms were present along the edges of the peatland. In the field, we observed some evidence of fire disturbance at this site, which could explain the absence of palms, since severe fires can inhibit palm regeneration (Huidobro et al., 2021). Fire history mapping using Earth observation data from sensors such as MODIS or VIIRS (Andela et al., 2022; Bolaño-Díaz et al., 2022) could be used to further explore this possibility. To assess the impact of fire over a longer time-frame (i.e., centuries to millennia), further field information such as the presence of charcoal in the upper soil layers would also be useful, as well as further investigation of the vegetation development of tropical peatland sites following a fire occurrence. Additionally, we obtained very good results in both low-statured white-sand ecosystems (cluster 1), and high-density (palm) swamps (cluster 2) with GEDI L2A rh95 data for canopy height. The use of in-situ canopy height instead of GEDI L2A rh95 further improved the prediction in the less densely vegetated white-sand ecosystems (cluster 1), although other in-situ variables showed no such effect. In cluster 2, the use of in-situ canopy height introduced large errors (Fig. S7a and b).

Furthermore, attention needs to be paid to the preparation of the data for the modeling process. It is important to note that we chose a threshold of −10 cm water level for our analysis. We selected this threshold as it describes the water level where the L-HH backscatter starts increasing compared to lower water levels, despite the limited ability of the SAR signal to deeply penetrate wet soil (Fig. S3, Fig. S4). We explain this with two phenomena. Firstly, below-ground water levels close to the surface lead to an increased surface soil moisture, which increases the SAR signal reflection. Thus, it is not surprising to see increases in L-HH backscatter with increased surface soil moisture. Secondly, the surface in these tropical peatland ecosystems is marked by very small-scale topographic variation, a complex mosaic of higher and lower lying areas (hummocks and hollows). It is thus not possible to clearly define one horizontal surface as “ground”. In the water level calibration, we used each well’s spatial position to calibrate to the ground level. Upscaling this point information to remote sensing pixels and image objects used in this study could introduce a bias, and water levels of a few cm below-ground could already inundate some low-lying areas within the image objects, leading to an increased double-bounce effect in the L-HH backscatter (Georgiou et al., 2023). Similarly, the increase in L-HH backscatter with rising water levels is explained by a water surface increasingly less interrupted by short vegetation and small-scale topographic variation.

Although we demonstrate some capacity to predict absolute water levels temporally from L-HH data for specific sites, we caution

that longer in-situ time-series are needed to assess its reliability across variable climatic conditions, including extreme events. Of all sites with linear correlations between water level and L-HH backscatter throughout the whole water level time-series, only four sites had linear correlations between the two variables in the two years independently. In 2019, the Loreto region experienced unusually high precipitation and water levels (Flores Llampazo et al., 2022; Griffis et al., 2020). Palm swamp QUI-01 is the only Peruvian site in our analysis that did not experience extreme flooding in 2019, and the water level variation in this site is not correlated with the river gauge (see Table 3 in Flores Llampazo et al. (2022)). The second Peruvian site with a significant linear correlation in both years despite high water levels in 2019, JEN-19 (orbit 137, 27° incidence angle), shows a large standard deviation $\sigma$ for 2019. This site had been identified as an outlier in cluster 2 and excluded from the multiple linear regression, it is thus questionable to what extent the individual year's linear regressions are representative of seasonally flooded forests. In Colombia, the palm swamp FDO-LPF (orbit 137 at 39° incidence angle), showed a linear correlation for 2024 data but not for 2023 data independently. The 2023/2024 hydrological year was drier than average in the Meta region (see 3.1). Both white-sand ecosystem sites with two years of water level data showed significant linear correlations between water level and L-HH backscatter in both years of water level data independently. Yet, a sample size of two is insufficient to draw conclusions on the applicability of this extrapolation to a larger area of white-sand ecosystems. With the temporal extrapolation working well in sites with similar water levels in both years, we hypothesize that extreme cases of water levels impeded linear correlations at the other sites. With more extreme water levels the correlation pattern of water level to L-HH backscatter might shift from linear to exponential or logarithmic, as the vegetation structure interacting with the SAR signal (i.e., above the water) changes. Longer in-situ time-series across sites with different vegetation structure and density are important to understand the L-band SAR backscatter response in extreme ENSO phases (and thus potentially extreme water levels) and changing climatic conditions.

To apply this approach in areas where no ecosystem or land cover map is available, our PCA can serve as a starting point for identifying suitable regions for monitoring above-ground water level dynamics with Earth observation. Although our method is not limited to peatland ecosystems, global peatland maps are useful for identifying regions with peatlands where monitoring water levels in relation to greenhouse gas emissions is particularly important.

### 4.3. Implications for carbon cycle modeling

In this study, we assessed the remote monitoring of neotropical peatland hydrology. Since hydrology is a primary control on GHG fluxes, our approach supports the incorporation of peatland ecosystems into local and regional GHG models, by providing spatially and temporally resolved information on water level variation. However, GHG flux modeling remains constrained by the limited availability of in-situ GHG measurements across these ecosystems. Although some measurements exist from palm swamp sites in Peru, especially QUI-01 (e.g., Griffis et al., 2020; Hergoualc'h et al., 2020), no flux data are available for Colombian sites. With this study, we offer a method to monitor water level variation, and also identify the vegetation structure of ecosystems with predictable correlations between water level and L-HH backscatter. Future work should prioritize GHG flux observations paired with water level data in ecosystems with suitable vegetation structure to inform C cycle modeling efforts using remote sensing.

Furthermore, we showed that the water levels in Colombian peatlands are moderately-well correlated to the water level of the nearby river, which aligns with findings from the Peruvian sites (Flores Llampazo et al., 2022). Thus, the river level could be used to predict peatland water level variation, offering a simpler approach than using L-band SAR backscatter. However, there are environmental and financial challenges involved with maintaining such a gauging station network. Regression-based predictions based on the current sparse networks of river stage levels do not capture water level variation across all sites within topographically complex floodplains. This challenge is best addressed through hydrological models, which simulate complex interactions among climate, vegetation, local topography, land use, soil attributes, and subsurface (lateral) flow processes, to predict water level dynamics. Modeling studies have shown how precipitation, evapotranspiration, and groundwater flow dictate water level dynamics, and how extreme climate events, artificial drainage, or land use changes drive seasonal, interannual and long-term trends in water level dynamics (Apers et al., 2022; Cobb et al., 2017; Mezbahuddin et al., 2015). The Surface Water and Ocean Topography (SWOT) mission, launched in 2022, is now providing unprecedented monitoring of terrestrial water bodies (global rivers > 100m wide, and lakes/ponds with surface area exceeding 250x250m$^2$, (NASA, 2024)). SWOT water surface height measurements have also been shown to be accurate for some types of vegetated wetlands (Kica et al., 2025). It is anticipated that future hydrologic modeling that assimilates SWOT, NISAR, and other satellite datasets will lead to improved capabilities for monitoring water levels in peatlands (Getirana et al., 2024).

Despite recent advances, hydrological modeling is still constrained by scarce field data, spatial variability in peat properties, and feedback between water levels, vegetation structure, and C fluxes. Some of the data needed for such modeling studies are not available for the sites in our analysis, such as high-resolution elevation information or data on subsurface flows. We thus argue that our approach using L-band SAR data is a valuable tool for monitoring spatial variability in water levels across different peatlands in remote tropical regions. However, vertical variation in water levels does not account for lateral flow, a pathway of dissolved organic C fluxes from the peatlands to the river (Griffis et al., 2020). Furthermore, the intensity of $CH_4$ fluxes is associated with the source of water input to tropical lowland peatlands (Finn et al., 2020). Thus, water level information alone is not sufficient to predict GHG fluxes from neotropical peatlands, but a combination of water level information with more comprehensive information on site vegetation, hydrology and climate, as well as corresponding GHG flux data from a larger number of sites for model training and validation would be necessary. Analysis of the relationships between the trophic status of peatlands, hydrology and GHG dynamics would be intrinsically valuable and would support linking hydrological or vegetation models to C cycle processes and inform large-scale land surface models.

## 5. Conclusion

In this study, we demonstrate the potential of combining L-band SAR data with vegetation structure information for monitoring tropical peatland water level dynamics. The sensitivity of the L-HH backscatter to water level variationswas explained largely by the vegetation structure, underscoring the importance of vegetation information when interpreting SAR signals in tropical swamp ecosystems. We used 20–30 m optical satellite data and a DEM-derived topographic measure to delineate areas of uniform peatland type and vegetation structure. Although some challenges remain, we demonstrate that L-band SAR HH backscatter is sensitive to changes in above-ground water levels in forested tropical white-sand and (palm) swamp ecosystems, which together form the largest part of peatland ecosystems in the study areas. Pole forests, where our approach failed, cover 11% of the Peruvian Amazon peatlands. Open palm swamps make up 11% and 6% of the peatlands in Peru and Colombia, respectively (Hastie et al., 2022; Uhde et al., 2025). Large-scale water level monitoring at a medium temporal scale should thus be feasible for these types of peatlands, using bi-weekly NISAR data.

Our findings further indicate that the water levels of our Colombian sites correlate more strongly with river stage than with local precipitation. Although this could imply that the peat sites receive water

inputmainly from the river, the hydrology can be complex and a correlation with river level does not necessarily mean surface water input. High river levels can create backwater effects, limiting peatland drainage and lateral fluxes. While river gauge data can serve as a general indicator of hydrological regimes, it lacks the spatial resolution needed for monitoring peatland water level dynamics at the ecosystem scale. The use of remote sensing data overcomes this limitation and enables consistent, spatially resolved monitoring of above-ground water level variations at centimeter variability.

Since water level variation is a primary control on GHG fluxes in these ecosystems, our study offers a pathway for incorporating spatially and temporally resolved hydrological information into regional GHG models. The ecosystem-specific differences in SAR sensitivity we identified suggest that a uniform representation of hydrological controls in carbon models may be insufficient. However, translating water level variation into meaningful estimates of GHG fluxes remains limited by the lack of concurrent in-situ flux data. A combination of hydrological dynamics with site-level GHG flux measurements is necessary to understand the impact of seasonal water level fluctuations—and long-term shifts therein—on regional C budgets. These measurements should be a research priority for upcoming investigations aiming to constrain the role of tropical peatlands in the global C cycle.

## CRediT authorship contribution statement

**Antje Uhde:** Writing – review & editing, Writing – original draft, Visualization, Validation, Software, Resources, Methodology, Investigation, Formal analysis, Data curation, Conceptualization. **Laura L. Hess:** Writing – review & editing, Resources, Methodology, Investigation, Data curation, Conceptualization. **Alison M. Hoyt:** Writing – review & editing, Supervision, Funding acquisition, Conceptualization. **Christiane Schmullius:** Writing – review & editing, Supervision, Project administration, Funding acquisition, Conceptualization. **Euridice N. Honorio Coronado:** Writing – review & editing, Investigation, Data curation, Conceptualization. **Edmundo Mendoza Olmos:** Writing – review & editing, Investigation. **Gerardo Flores Llampazo:** Writing – review & editing, Investigation. **Susan Trumbore:** Writing – review & editing, Supervision, Funding acquisition, Conceptualization. **Timothy Baker:** Writing – review & editing, Investigation. **Juan S. Hernandez Suarez:** Writing – review & editing. **Oliver L. Phillips:** Writing – review & editing, Investigation, Data curation. **Frederick C. Draper:** Writing – review & editing, Investigation. **Andrés G. Hernandez Ortega:** Writing – review & editing, Investigation. **Luis A. Torres-Montenegro:** Writing – review & editing, Investigation. **R. Scott Winton:** Writing – review & editing, Supervision, Resources, Project administration, Methodology, Investigation, Funding acquisition, Data curation, Conceptualization.

## Declaration of competing interest

The authors declare the following financial interests/personal relationships that may be considered as potential competing interests:

Antje Uhde reports that financial support was provided by the International Max Planck Research School for Global Biogeochemical Cycles. Alison M. Hoyt, and R. Scott Winton report that financial support was provided by the Stanford University King Center on Global Development. R. Scott Winton reports that financial support was provided by the Swiss National Science Foundation. Alison M. Hoyt reports that financial support was provided by the National Science Foundation. Laura Hess reports that financial support was provided by BNP Paribas. Timothy Baker reports that financial support was provided by the Gordon and Betty Moore Foundation. Euridice N. Honorio Coronado reports that financial support was provided by UK Research and Innovation Natural Environment Research Council. If there are other authors, they declare that they have no known competing financial interests or personal relationships that could have appeared to influence the work reported in this paper.

## Acknowledgments

AU received funding from the International Max Planck Research School for global Biogeochemical Cycles. The work was supported by the King Center on Global Development at Stanford University (AMH, RSW); a Spark grant from the Swiss National Science Foundation (Project CRSK-2 190328) (RSW); the National Science Foundation under Grant 2406964 (AMH); a BNP Paribas (France) Climate and Biodiversity Initiative award (SABERES: Sustaining Amazon Floodplain Biodiversity and Fisheries under Climate Change), and The Gordon and Betty Moore Foundation (grant number 5349, 'MonANPeru'). E.N.H.C. acknowledges support from her NERC Knowledge Exchange Fellowship (NE/V018760/2).

We thank the NGO Horizonte Verde for the Colombia field campaign support. This publication is based on Research Project '259. Monitoring water level dynamics in tropical forest peatlands from space' of the ForestPlots.net global collaboration. We thank the administration of the ForestPlots.net database for their support. We acknowledge and are very grateful for the data collected in the field and shared by J. F. Restrepo Cañola, C. Ballón Falcón, J. C. Cordova Oroche, M. Corrales Medina, D. Galiano Cabrera, J. M. Grandez Rios, G. Hidalgo Pinzango, C. P. Perez Macedo, J. Reyna Huaymacari, M. A. Ríos Paredes, and K. H. Roucoux. We would also like to thank the anonymous reviewers for their time and effort. Their comments and remarks have greatly helped to improve the clarity, precision and relevance of our manuscript.

During the preparation of this work the author(s) used ChatGPT and Grammarly to improve the readability of this manuscript. After using these tools/services, the author(s) reviewed and edited the content as needed and take(s) full responsibility for the content of the publication.

## Appendix A. Supplementary data

Supplementary data for this article can be found online at doi:10.1016/j.rse.2026.115342.

## Data availability

Data will be made available on request.

## References

Andela, N., Morton, D.C., Schroeder, W., Chen, Y., Brando, P.M., Randerson, J.T., 2022. Tracking and classifying Amazon fire events in near real time. Sci. Adv. 8, eabd2713. https://doi.org/10.1126/sciadv.abd2713

Apers, S., De Lannoy, G.J.M., Baird, A.J., Cobb, A.R., Dargie, G.C., del Aguila Pasquel, J., Gruber, A., Hastie, A., Hidayat, H., Hirano, T., Hoyt, A.M., Jovani-Sancho, A.J., Katimon, A., Kurnain, A., Koster, R.D., Lampela, M., Mahanama, S.P.P., Melling, L., Page, S.E., Reichle, R.H., Taufik, M., Vanderborght, J., Bechtold, M., de Lannoy, G.J.M., Pasquel, J., Jovani–Sancho, A.J., 2022. Tropical peatland Hydrology simulated with a global land surface model. J. Adv. Model. Earth Syst. 14, https://doi.org/10.1029/2021MS002784

Beck, H.E., Wood, E.F., Pan, M., Fisher, C.K., Miralles, D.G., van Dijk, A.I.J.M., McVicar, T.R., Adler, R.F., 2019. MSWEP v2 global 3-hourly 0.1Â° precipitation: methodology and quantitative assessment. Bull. Am. Meteorol. Soc. 100, 473–500. https://doi.org/10.1175/BAMS-D-17-0138.1

Bettinger, P., Boston, K., Siry, J.P., Grebner, D.L., 2017. Valuing and characterizing forest conditions. In: Bettinger, P., Boston, K., Siry, J.P., Grebner, D.L. (Eds.), Forest Management and Planning. Elsevier, pp. 21–63. https://doi.org/10.1016/B978-0-12-809476-1.00002-3

Bolaño-Díaz, S., Camargo-Caicedo, Y., Soro, T.D., N'Dri, A.B., Bolaño-Ortiz, T.R., 2022. Spatio-Temporal characterization of fire using MODIS data (2000–2020) in Colombia. Fire 5, 134. https://doi.org/10.3390/fire5050134

Bourgeau-Chavez, L.L., Grelik, S.L., Battaglia, M.J., Leisman, D.J., Chimner, R.A., Hribljan, J.A., Lilleskov, E.A., Draper, F.C., Zutta, B.R., Hergoualc'h, K., Bhomia, R.K., Lähteenoja, O., 2021. Advances in amazonian peatland discrimination with Multi-Temporal PALSAR refines estimates of peatland distribution, c stocks and deforestation. Front. Earth Sci. 9, https://doi.org/10.3389/feart.2021.676748

Burdun, I., Bechtold, M., Aurela, M., de Lannoy, G., Desai, A.R., Humphreys, E., Kareksela, S., Komisarenko, V., Liimatainen, M., Marttila, H., Minkkinen, K., Nilsson, M.B., Ojanen, P., Salko, S.-S., Tuittila, E.-S., Uuemaa, E., Rautiainen, M., 2023. Hidden becomes clear: optical remote sensing of vegetation reveals water table dynamics in northern peatlands. Remote Sens. Environ. 296, 113736. https://doi.org/10.1016/j.rse.2023.113736

Carlson, K.M., Goodman, L.K., May-Tobin, C.C., 2015. Modeling relationships between water table depth and peat soil carbon loss in southeast asian plantations. Environ. Res. Lett. 10, 074006. https://doi.org/10.1088/1748-9326/10/7/074006

Chapman, B., McDonald, K., Shimada, M., Rosenqvist, A., Schroeder, R., Hess, L., 2015. Mapping regional inundation with spaceborne L-Band SAR. Remote Sens. 7, 5440–5470. https://doi.org/10.3390/rs70505440

Chave, J., Réjou-Méchain, M., Búrquez, A., Chidumayo, E., Colgan, M.S., Delitti, W.B.C., Duque, A., Eid, T., Fearnside, P.M., Goodman, R.C., Henry, M., Martínez-Yrízar, A., Mugasha, W.A., Muller-Landau, H.C., Mencuccini, M., Nelson, B.W., Ngomanda, A., Nogueira, E.M., Ortiz-Malavassi, E., Pélissier, R., Ploton, P., Ryan, C.M., Saldarriaga, J.G., Vieilledent, G., 2014. Improved allometric models to estimate the aboveground biomass of tropical trees. Glob. Change Biol. 20, 3177–3190. https://doi.org/10.1111/gcb.12629

Cobb, A.R., Hoyt, A.M., Gandois, L., Eri, J., Dommain, R., Abu Salim, K., Kai, F.M., Haji Su'ut, N.S., Harvey, C.F., 2017. How temporal patterns in rainfall determine the geomorphology and carbon fluxes of tropical peatlands. Proc. Natl. Acad. Sci. U.S.A. 114, E5187–E5196. https://doi.org/10.1073/pnas.1701090114

Copernicus Contributing Missions Online, 2022. Copernicus DEM. https://dataspace.copernicus.eu/explore-data/data-collections/copernicus-contributing-missions/collections-description/COP-DEM.

Couwenberg, J., Dommain, R., Joosten, H., 2010. Greenhouse gas fluxes from tropical peatlands in south–east Asia. Glob. Change Biol. 16, 1715–1732. https://doi.org/10.1111/j.1365-2486.2009.02016.x

Dargie, G.C., Lewis, S.L., Lawson, I.T., Mitchard, E.T.A., Page, S.E., Bocko, Y.E., Ifo, S.A., 2017. Age, extent and carbon storage of the central Congo basin peatland complex. Nature 542, 86–90. https://doi.org/10.1038/nature21048

Draper, F.C., Honorio Coronado, E.N., Roucoux, K.H., Lawson, I.T., Pitman, N.C., Fine, P.V., Phillips, O.L., Torres Montenegro, L.A., Valderrama Sandoval, E., Mesones, I., García–Villacorta, R., Arévalo, F.R.R., Baker, T.R., 2018. Peatland forests are the least diverse tree communities documented in amazonia, but contribute to high regional beta–diversity. Ecography 41, 1256–1269. https://doi.org/10.1111/ecog.03126

Draper, F.C., Roucoux, K.H., Lawson, I.T., Mitchard, E.T.A., Honorio Coronado, E.N., Lähteenoja, O., Torres Montenegro, L., Valderrama Sandoval, E., Zaráte, R., Baker, T.R., 2014. The distribution and amount of carbon in the largest peatland complex in amazonia. Environ. Res. Lett. 9, 124017. https://doi.org/10.1088/1748-9326/9/12/124017

Drusch, M., Del Bello, U., Carlier, S., Colin, O., Fernandez, V., Gascon, F., Hoersch, B., Isola, C., Laberinti, P., Martimort, P., Meygret, A., Spoto, F., Sy, O., Marchese, F., Bargellini, P., 2012. Sentinel-2: ESA's optical High-Resolution mission for GMES operational services. Remote Sens. Environ. 120, 25–36. https://doi.org/10.1016/j.rse.2011.11.026

Dubayah, R., Blair, J.B., Goetz, S., Fatoyinbo, L., Hansen, M., Healey, S., Hofton, M., Hurtt, G., Kellner, J., Luthcke, S., Armston, J., Tang, H., Duncanson, L., Hancock, S., Jantz, P., Marselis, S., Patterson, P.L., Qi, W., Silva, C., 2020. The global ecosystem dynamics investigation: high-resolution laser ranging of the earth's forests and topography. Sci. Remote Sens. 1, 100002. https://doi.org/10.1016/j.srs.2020.100002

Finn, D.R., Ziv-El, M., van Haren, J., Park, J.G., Del Aguila-Pasquel, J., Urquiza-Muñoz, J.D., Cadillo-Quiroz, H., 2020. Methanogens and methanotrophs show Nutrient-Dependent community assemblage patterns across tropical peatlands of the Pastaza-Marañón basin, Peruvian amazonia. Front. Microbiol. 11, 746. https://doi.org/10.3389/fmicb.2020.00746

Flores Llampazo, G., Honorio Coronado, E.N., Del Aguila–Pasquel, J., Cordova Oroche, C.J., Díaz Narvaez, A., Reyna Huaymacari, J., Grandez Ríos, J., Lawson, I.T., Hastie, A., Baird, A.J., Baker, T.R., 2022. The presence of peat and variation in tree species composition are under different hydrological controls in amazonian wetland forests. Hydrol. Process. 36, https://doi.org/10.1002/hyp.14690

ForestPlots.net. Database. www.ForestPlots.net.

ForestPlots.net, Blundo, C., Carilla, J., Grau, R., Malizia, A., Malizia, L., Osinaga-Acosta, O., Bird, M., Bradford, M., Catchpole, D., Ford, A., Graham, A., Hilbert, D., Kemp, J., Laurance, S., Laurance, W., Ishida, F.Y., Marshall, A., Waite, C., Woell, H., et al., 2021. Taking the pulse of earth's tropical forests using networks of highly distributed plots. Biol. Conserv. 260, 108849. https://doi.org/10.1016/j.biocon.2020.108849

Georgiou, S., Mitchard, E.T.A., Crezee, B., Dargie, G.C., Young, D.M., Jovani-Sancho, A.J., Kitambo, B., Papa, F., Bocko, Y.E., Bola, P., Crabtree, D.E., Emba, O.B., Ewango, C.E.N., Girkin, N.T., Ifo, S.A., Kanyama, J.T., Mampouya, Y.E.W., Mbemba, M., Ndjango, J.-B.N., Palmer, P.I., Sjögersten, S., Lewis, S.L., 2023. Mapping water levels across a region of the cuvette centrale peatland complex. Remote Sens. 15, 3099. https://doi.org/10.3390/rs15123099

Getirana, A., Kumar, S., Bates, P., Boone, A., Lettenmaier, D., Munier, S., 2024. The SWOT mission will reshape our understanding of the global terrestrial water cycle. Nature Water 2, 1139–1142. https://doi.org/10.1038/s44221-024-00352-0

Goldstein, A., Turner, W.R., Spawn, S.A., Anderson-Teixeira, K.J., Cook-Patton, S., Fargione, J., Gibbs, H.K., Griscom, B., Hewson, J.H., Howard, J.F., Ledezma, J.C., Page, S., Koh, L.P., Rockström, J., Sanderman, J., Hole, D.G., 2020. Protecting irrecoverable carbon in earth's ecosystems. Nat. Clim. Change 10, 287–295. https://doi.org/10.1038/s41558-020-0738-8

Goodman, R.C., Phillips, O.L., Del Castillo Torres, D., Freitas, L., Cortese, S.T., Monteagudo, A., Baker, T.R., 2013. Amazon palm biomass and allometry. For. Ecol. Manag. 310, 994–1004. https://doi.org/10.1016/j.foreco.2013.09.045

Google for Developers, 2024. PALSAR-2 ScanSAR level 2.2 | earth engine data catalog | Google for developers. https://developers.google.com/earth-engine/datasets/catalog/JAXA_ALOS_PALSAR-2_Level2_2_ScanSAR.

Griffis, T.J., Roman, D.T., Wood, J.D., Deventer, J., Fachin, L., Rengifo, J., Del Castillo, D., Lilleskov, E., Kolka, R., Chimner, R.A., Del Aguila-Pasquel, J., Wayson, C., Hergoualc'h, K., Baker, J.M., Cadillo-Quiroz, H., Ricciuto, D.M., 2020. Hydrometeorological sensitivities of net ecosystem carbon dioxide and methane exchange of an amazonian palm swamp peatland. Agric. For. Meteorol. 295, 108167. https://doi.org/10.1016/j.agrformet.2020.108167

Gumbricht, T., Roman-Cuesta, R.M., Verchot, L., Herold, M., Wittmann, F., Householder, E., Herold, N., Murdiyarso, D., 2017. An expert system model for mapping tropical wetlands and peatlands reveals south america as the largest contributor. Glob. Change Biol. 23, 3581–3599. https://doi.org/10.1111/gcb.13689

Hastie, A., Honorio Coronado, E.N., Reyna, J., Mitchard, E.T.A., Åkesson, C.M., Baker, T.R., Cole, L.E.S., Oroche, C.J.C., Dargie, G., Dávila, N., de Grandi, E.C., Del Águila, J., Del Castillo Torres, D., de La Cruz Paiva, R., Draper, F.C., Flores, G., Grández, J., Hergoualc'h, K., Householder, J.E., Janovec, J.P., Lähteenoja, O., Reyna, D., Rodríguez-Veiga, P., Roucoux, K.H., Tobler, M., Wheeler, C.E., Williams, M., Lawson, I.T., 2022. Risks to carbon storage from land-use change revealed by peat thickness maps of Peru. Nat. Geosci. 15, 369–374. https://doi.org/10.1038/s41561-022-00923-4

Hastie, A., Householder, J.E., Honorio Coronado, E.N., Hidalgo Pizango, C.G., Herrera, R., Lähteenoja, O., de Jong, J., Winton, R.S., Aymard Corredor, G.A., Reyna, J., Montoya, E., Paukku, S., Mitchard, E.T.A., Åkesson, C.M., Baker, T.R., Cole, L.E.S., Córdova Oroche, C.J., Dávila, N., Del Águila, J., Draper, F.C., Fluet-Chouinard, E., Grández, J., Janovec, J.P., Reyna, D., Tobler, M., Del Castillo Torres, D., Roucoux, K.H., Wheeler, C.E., Fernandez Piedade, M.T., Schöngart, J., Wittmann, F., van der Zon, M., Lawson, I.T., 2024. A new data-driven map predicts substantial undocumented peatland areas in amazonia. Environ. Res. Lett. 19, 094019. https://doi.org/10.1088/1748-9326/ad677b

Hergoualc'h, K., Dezzeo, N., Verchot, L.V., Martius, C., van Lent, J., Del Aguila-Pasquel, J., López Gonzales, M., 2020. Spatial and temporal variability of soil $n_2$ o and $CH_4$ fluxes along a degradation gradient in a palm swamp peat forest in the Peruvian Amazon. Glob. Change Biol. 26, 7198–7216. https://doi.org/10.1111/gcb.15354

Hergoualc'h, K., van Lent, J., Dezzeo, N., Verchot, L.V., van Groenigen, J.W., López Gonzales, M., Grandez-Rios, J., 2024. Major carbon losses from degradation of mauritia flexuosa peat swamp forests in western amazonia. Biogeochemistry 167, 327–345. https://doi.org/10.1007/s10533-023-01057-4

Hersbach, H., Bell, B., Berrisford, P., Hirahara, S., Horányi, A., Muñoz–Sabater, J., Nicolas, J., Peubey, C., Radu, R., Schepers, D., Simmons, A., Soci, C., Abdalla, S., Abellan, X., Balsamo, G., Bechtold, P., Biavati, G., Bidlot, J., Bonavita, M., de Chiara, G., Dahlgren, P., Dee, D., Diamantakis, M., Dragani, R., Flemming, J., Forbes, R., Fuentes, M., Geer, A., Haimberger, L., Healy, S., Hogan, R.J., Hólm, E., Janisková, M., Keeley, S., Laloyaux, P., Lopez, P., Lupu, C., Radnoti, G., de Rosnay, P., Rozum, I., Vamborg, F., Villaume, S., Thépaut, J.-N., 2020. The ERA5 global reanalysis. Q. J. R. Meteorol. Soc. 146, 1999–2049. https://doi.org/10.1002/qj.3803

Hess, L., Durieux, L., 2026. Relative terrain height DEM transform for the mid-juruá region, Brazilian Amazon. Dataset. https://doi.org/10.5061/dryad.wstqjq314

Hess, L., Melack, J.L., Novo, E.M., Barbosa, C.C.F., Gastil, M., 2003. Dual-season mapping of wetland inundation and vegetation for the central Amazon basin. Remote Sens. Environ. 87, 404–428. https://doi.org/10.1016/j.rse.2003.04.001

Hirano, T., Jauhiainen, J., Inoue, T., Takahashi, H., 2009. Controls on the carbon balance of tropical peatlands. Ecosystems 12, 873–887. https://doi.org/10.1007/s10021-008-9209-1

Hirano, T., Segah, H., Kusin, K., Limin, S., Takahashi, H., Osaki, M., 2012. Effects of disturbances on the carbon balance of tropical peat swamp forests. Glob. Change Biol. 18, 3410–3422. https://doi.org/10.1111/j.1365-2486.2012.02793.x

Honorio Coronado, E.N., Hastie, A., Reyna, J., Flores, G., Grández, J., Lähteenoja, O., Draper, F.C., Åkesson, C.M., Baker, T.R., Bhomia, R.K., Cole, L.E.S., Dávila, N., Del Águila, J., Del Águila, M., Del Castillo Torres, D., Lawson, I.T., Martín Brañas, M., Mitchard, E.T.A., Monteagudo, A., Phillips, O.L., Ramírez, E., Ríos, M., Ríos, S., Rodriguez, L., Roucoux, K.H., Tagle Casapia, X., Vasquez, R., Wheeler, C.E., Montoya, M., 2021. Intensive field sampling increases the known extent of carbon-rich amazonian peatland pole forests. Environ. Res. Lett. 16, 074048. https://doi.org/10.1088/1748-9326/ac0e65

Hoyos-Santillan, J., Lomax, B.H., Large, D., Turner, B.L., Lopez, O.R., Boom, A., Sepulveda-Jauregui, A., Sjögersten, S., 2019. Evaluation of vegetation communities, water table, and peat composition as drivers of greenhouse gas emissions in lowland tropical peatlands. Sci. Total Environ. 688, 1193–1204. https://doi.org/10.1016/j.scitotenv.2019.06.366

Hoyt, A.M., Gandois, L., Eri, J., Kai, F.M., Harvey, C.F., Cobb, A.R., 2019. $CO_2$ emissions from an undrained tropical peatland: interacting influences of temperature, shading and water table depth. Glob. Change Biol. 25, 2885–2899. https://doi.org/10.1111/gcb.14702

Huidobro, G., Bernal, R., Wagner, S., 2021. Post-fire regeneration of the palm mauritia flexuosa in vichada, Orinoco region of Colombia. In: Leal Filho, W., Azeiteiro, U.M., Setti, A.F.F. (Eds.), Sustainability in Natural Resources Management and Land Planning. Springer International Publishing and Imprint Springer, Cham. World Sustainability Series, pp. 445–463. https://doi.org/10.1007/978-3-030-76624-526

IDEAM, 2024. Consulta y descarga de datos hidrometeorológicos. Website. http://dhime.ideam.gov.co/atencionciudadano/.

Irons, J.R., Dwyer, J.L., Barsi, J.A., 2012. The next landsat satellite: the landsat data continuity mission. Remote Sens. Environ. 122, 11–21. https://doi.org/10.1016/j.rse.2011.08.026

Kalacska, M., Arroyo-Mora, J., Soffer, R., Roulet, N., Moore, T., Humphreys, E., Leblanc, G., Lucanus, O., Inamdar, D., 2018. Estimating peatland water table depth and net ecosystem exchange: a comparison between satellite and airborne imagery. Remote Sens. 10, 687. https://doi.org/10.3390/rs10050687

Kica, S., Pavelsky, T.M., Fayne, J.V., Williams, B.A., 2025. SWOT water surface elevation in herbaceous wetlands of florida's everglades. Geophys. Res. Lett. 52, https://doi.org/10.1029/2025GL114956

Kimmel, K., Mander, Ü., 2010. Ecosystem services of peatlands: implications for restoration. Prog. Phys. Geogr. Earth Environ. 34, 491–514. https://doi.org/10.1177/0309133310365595

Kojima, Y., Oki, K., Noborio, K., Mizoguchi, M., 2016. Estimating soil moisture distributions across small farm fields with ALOS/PALSAR. Int. Sch. Res. Not. 2016, 4203783. https://doi.org/10.1155/2016/4203783

Lähteenoja, O., Ruokolainen, K., Schulman, L., Oinonen, M., 2009. Amazonian peatlands: an ignored c sink and potential source. Glob. Change Biol. 15, 2311–2320. https://doi.org/10.1111/j.1365-2486.2009.01920.x

Le Toan, T., Quegan, S., Davidson, M.W.J., Balzter, H., Paillou, P., Papathanassiou, K., Plummer, S., Rocca, F., Saatchi, S., Shugart, H., Ulander, L., 2011. The BIOMASS mission: mapping global forest biomass to better understand the terrestrial carbon cycle. Remote Sens. Environ. 115, 2850–2860. https://doi.org/10.1016/j.rse.2011.03.020

Lee, H., Yuan, T., Jung, H.C., Beighley, E., 2015. Mapping wetland water depths over the central Congo basin using PALSAR ScanSAR, envisat altimetry, and MODIS VCF data. Remote Sens. Environ. 159, 70–79. https://doi.org/10.1016/j.rse.2014.11.030

Lopez–Gonzalez, G., Lewis, S.L., Burkitt, M., Phillips, O.L., 2011. ForestPlots.net: a web application and research tool to manage and analyse tropical forest plot data. J. Veg. Sci. 22, 610–613. https://doi.org/10.1111/j.1654-1103.2011.01312.x

Loveland, T.R., Dwyer, J.L., 2012. Landsat: building a strong future. Remote Sens. Environ. 122, 22–29. https://doi.org/10.1016/j.rse.2011.09.022

Luckman, A., Baker, J., Kuplich, T.M., da Costa Freitas Yanasse, C., Frery, A.C., 1997. A study of the relationship between radar backscatter and regenerating tropical forest biomass for spaceborne SAR instruments. Remote Sens. Environ. 60, 1–13. https://doi.org/10.1016/S0034-4257(96)00121-6

Mermoz, S., Le Toan, T., Villard, L., Réjou-Méchain, M., Seifert-Granzin, J., 2014. Biomass assessment in the Cameroon savanna using ALOS PALSAR data. Remote Sens. Environ. 155, 109–119. https://doi.org/10.1016/j.rse.2014.01.029

Mezbahuddin, M., Grant, R.F., Hirano, T., 2015. How Hydrology determines seasonal and interannual variations in water table depth, surface energy exchange, and water stress in a tropical peatland: modeling versus measurements. J. Geophys. Res.: Biogeosci. 120, 2132–2157. https://doi.org/10.1002/2015JG003005

Minasny, B., Adetsu, D.V., Aitkenhead, M., Artz, R.R.E., Baggaley, N., Barthelmes, A., Beucher, A., Caron, J., Conchedda, G., Connolly, J., Deragon, R., Evans, C., Fadnes, K., Fiantis, D., Gagkas, Z., Gilet, L., Gimona, A., Glatzel, S., Greve, M.H., Habib, W., Hergoualc'h, K., Hermansen, C., Kidd, D.B., Koganti, T., Kopansky, D., Large, D.J., Larmola, T., Lilly, A., Liu, H., Marcus, M., Middleton, M., Morrison, K., Petersen, R.J., Quaife, T., Rochefort, L., Rudiyanto, Toca, L., Tubiello, F.N., Weber, P.L., Weldon, S., Widyatmanti, W., Williamson, J., Zak, D., 2023. Mapping and monitoring peatland conditions from global to field scale. Biogeochemistry 167, 383–425. https://doi.org/10.1007/s10533-023-01084-1

NASA, 2024. SWOT science data products user handbook. https://www.earthdata.nasa.gov/s3fs-public/2024-06/D-109532_SWOT_UserHandbook_20240502.pdf.

NISAR, 2018. NASA-ISRO SAR (NISAR) Mission Science Users' Handbook. NASA Jet Propulsion Laboratory.

Oakes, G., Hardy, A., Bunting, P., Rosenqvist, A., 2024. RadWet-L: a novel approach for mapping of inundation dynamics of forested wetlands using ALOS-2 PALSAR-2 L-Band radar imagery. Remote Sens. 16, 2078. https://doi.org/10.3390/rs16122078

Palomino–Ángel, S., Wdowinski, S., Li, S., 2024. Wetlands water level measurements from the new generation of satellite laser altimeters: systematic spatial–temporal evaluation of ICESat–2 and GEDI missions over the south Florida everglades. Water Resour. Res. 60, https://doi.org/10.1029/2023WR035422

Rieley, J.O., Wüst, R.A.J., Jauhiainen, J., Page, S.E., Wösten, J.H.M., Hooijer, A., Siegert, E., Limin, S.H., Vasander, H., Stahlhut, M., 2008. Tropical peatlands: carbon stores, carbon gas emissions and contribution to climate change processes. Peatlands and climate change. https://api.semanticscholar.org/CorpusID:140191433.

Rosenqvist, A., Shimada, M., Suzuki, S., Ohgushi, F., Tadono, T., Watanabe, M., Tsuzuku, K., Watanabe, T., Kamijo, S., Aoki, E., 2014. Operational performance of the ALOS global systematic acquisition strategy and observation plans for ALOS-2 PALSAR-2. Remote Sens. Environ. 155, 3–12. https://doi.org/10.1016/j.rse.2014.04.011

Rouse Jr., J.W., Haas, R.H., Schell, J.A., Deering, D.W., 1974. Monitoring vegetation systems in the great plains with ERTS. Goddard Space Flight Center 3d ERTS-1 Symp. 1.

Saatchi, S., Marlier, M., Chazdon, R.L., Clark, D.B., Russell, A.E., 2011. Impact of spatial variability of tropical forest structure on radar estimation of aboveground biomass. Remote Sens. Environ. 115, 2836–2849. https://doi.org/10.1016/j.rse.2010.07.015

Trimble Germany GmbH, 1995–2022. eCognition developer. Software.

Tsyganskaya, V., Martinis, S., Marzahn, P., Ludwig, R., 2018. SAR-based detection of flooded vegetation – a review of characteristics and approaches. Int. J. Remote Sens. 39, 2255–2293. https://doi.org/10.1080/01431161.2017.1420938

Uhde, A., Hoyt, A.M., Hess, L., Schmullius, C., Mendoza, E., Benavides, J.C., Trumbore, S., Martín–López, J.M., Skillings–Neira, P.N., Winton, R.S., 2025. Mapping peatland distribution and quantifying peatland below–ground carbon stocks in colombia's eastern lowlands. J. Geophys. Res.: Biogeosci. 130, https://doi.org/10.1029/2024JG008505

Ulaby, F.T., Dubois, P.C., van Zyl, J., 1996. Radar mapping of surface soil moisture. J. Hydrol. 184, 57–84. https://doi.org/10.1016/0022-1694(95)02968-0

UNEP, 2022. Global Peatlands Assessment - the State of the World's Peatlands: Evidence for Action Toward the Conservation, Restoration, and Sustainable Management of Peatlands: Main Report. Nairobi.

Wang, Y., Davis, F.W., Melack, J.M., Kasischke, E.S., Christensen, N.L., 1995a. The effects of changes in forest biomass on radar backscatter from tree canopies. Int. J. Remote Sens. 16, 503–513. https://doi.org/10.1080/01431169508954415

Wang, Y., Hess, L.L., Filoso, S., Melack, J.M., 1995b. Understanding the radar backscattering from flooded and nonflooded amazonian forests: results from canopy backscatter modeling. Remote Sens. Environ. 54, 324–332. https://doi.org/10.1016/0034-4257(95)00140-9

Winton, R.S., Benavides, J., Mendoza, E., Uhde, A., Hastie, A., Honorio Coronado, E., Hernandez Ortega, A.G., Paukku, S., Mullins, B., Del Aguila Pasquel, J., Aymard Corredor, G.A., Baker, T., Draper, F., Flores Llampazo, G., Herrera, R., Phillips, O.L., Reyna Huaymacari, J., ter Steege, H., Stropp, J., Lawson, I.T., Gallego-Sala, A.V., Boom, A., Wehrli, B., Hoyt, A.M., 2025. Widespread carbon-dense peatlands in the Colombian lowlands. Environ. Res. Lett.. https://doi.org/10.1088/1748-9326/adbc03

Wüst, R.A.J., Bustin, M., Lavkulich, L.M., 2003. New classification systems for tropical organic-rich deposits based on studies of the tasek bera basin, Malaysia. CATENA 53, 133–163. https://doi.org/10.1016/S0341-8162(03)00022-5

Zanne, A.E., Lopez-Gonzalez, G., Coomes, D.A., Ilic, J., Jansen, S., Lewis, S.L., Miller, R.B., Swenson, N.G., Wiemann, M.C., Chave, J., 2009. Global wood density database. https://doi.org/10.5061/DRYAD.234

Zhou, X., Wang, J., Shan, B., He, Y., Xing, M., 2025. Sensitivity of multi-frequency and multi-polarization SAR to soil moisture at different depths in agricultural regions. J. Hydrol. 660, 133513. https://doi.org/10.1016/j.jhydrol.2025.133513